Journal of Thermal Analysis and Calorimetry (2026) 151:9295–9313
https://doi.org/10.1007/s10973-026-15428-0

Nonlinear thermophysical dynamics of MHD hybrid nanofluids: a multiparametric fractional framework assisted by artificial neural networks

Shajar Abbas[1,2] · Muhammad Ramzan[3] · Rashid Jan[4] · Assmaa Abd-Elmonem[5] · Mawadda E. E. Abulhassan[5] · Ilkhom Khaydarov[6] · Mehrigul Hayitova[7] · Ibrahim Mahariq[8,9,10,11,12]

Received: 8 January 2026 / Accepted: 27 February 2026 / Published online: 30 March 2026

Abstract
The study of non-Newtonian fluids has drawn much scholarly attention because of the wide range of applications they have in industrial processes, such as plastic, lubrication systems, and in mining operations. When combined with magnetohydrodynamic effects their importance widens to more advanced technological and biomedical applications such as magnetic resonance imaging, medical diagnostics, and hyperthermia treatment. Recent investigations have proven that the addition of nanosized particles into base fluids improves the thermal performance and the heat transfer efficiency. Nevertheless, heat transfer in realistic mechanical systems is affected by a huge number of interacting physical parameters, each with different contribution to overall behavior. In the present study, a sensitivity analysis is conducted to study the effect of some important parameters, which include internal heat generation, magnetic field strength, and Casson nanofluid properties. The governing equations are derived from fundamental conservation laws and transformed into a dimensionless form for generalization. The model is generalized by using Fourier's and Fick's laws. Analytical treatment is achieved using the Laplace transform technique, while the Levenberg–Marquardt algorithm is employed for numerical prediction and validation. Results demonstrate high accuracy with mean-squared error values below 10^{-10} especially for a fractional nanofluid Casson flow model. The Levenberg–Marquardt algorithm is utilized, with 70% of the data used for training and 15% allocated for validation and testing. The findings reveal that momentum increases with decreasing fractional parameters. Table 4 gives the validity of present work with already published work.

Keywords Laplace transform method · Magnetic field · Nanoparticles · Fractional derivatives · Neural networks · Heat transfer · Mass transfer · Casson fluid, porous media · Chemical reaction · Suction/injection · Levenberg–Marquardt algorithm.

List of symbols

γ,	Fractional parameters
q	Laplace transform variables
η	Casson parameter
T	Dimensionless temperature
Gr	Thermal Grashof number
Pr	Prandtl number
y	Perpendicular axis
σ	Electrical conductivity
B_0	Magnetic field parameter
S	Suction parameter
M	Magnetic parameter
C	Dimensionless concentration
Gm	Mass Grashof number
Sc	Schmidt number
x	A dimensionless coordinate axis along the plate

Extended author information available on the last page of the article

Introduction

Analytical assessment of system responsiveness plays a crucial role in manufacturing processes to evaluate the influence of diverse input parameters on various fluid flow phenomena. This technique has become integral to contemporary theoretical and industrial advancements, particularly in the optimization of control mechanisms across different engineering domains. Beyond its primary applications, such evaluations have extended their impact into numerous scientific disciplines, including nuclear engineering, ecological studies, biomedicine, and socio-economic research. In order to check the effective responses of the system, it is necessary to established a significant interdependencies among the factors of input and behavior of output. To explain such type of connection, many researcher investigated different types of operators/methods. The formulation/connection of correlation is the most important/emerging strategies in these research/techniques. This method/technique evaluate/verified the relationship between physical parameters/quantities in engineering discipline and applied sciences. Several scholars studied/evaluated the computational, numerical, or analytical technique/methods to worked on problems/models as given in [1–7].

There are two types of fluid, one is classical Newtonian fluid, and other is non-Newtonian. These two fluids differ due to the viscosity property which indicate the flow properties. This flow property have unique behavior to differ them in the mechanisms of lubrication, synthesis of polymer, biomedical discipline, chemical process, applied physics, applied mathematics, aerodynamic system, material system, industrial and engineering process. Due to technical importance/significance in these systems, these fluid have obtained a crucial momentum. In order to evaluate these problems, many researcher worked on it. the influence of Caputo operator on MHD flow of fluid is evaluated by Asjad et al. [8]. Ramzan et al. [9] investigated the channel flow of Casson fluid via Laplace and fractional operator. Krishna et al. [10] proposed an analytical approach for fluid motion in parallel plates with thermal effects. Samniulaga et al. [11] examined the viscous flow of fluid with heat flux and temperature distribution, whereas Sheikh et al. [12] observed the unsteady flow of second grade fluid with modern fractional operator. Kataria et al. [13] investigated thermochemical diffusion effects in unsteady magnetohydrodynamic (MHD) motion past a vertically oscillating plate, while Shah et al. [14] proposed a semi-analytical framework for solving fractional-order Navier–Stokes equations.

This memory effect is very important for effectively simulating physical, biological, and economic systems including viscoelastic materials, anomalous diffusion, and financial markets, where what happened in the past has a big impact on what happens now. Fractional calculus has gained great prominence in the research of fluid mechanics due to its versatile applicability. For example, Sene [15] used a fractionalized Caputo operator to study the flow of viscous Newtonian fluids, while Razzaque and colleagues [16] examined the effect of fractional-based thermal and mass diffusion. Chu et al. [17] created an analytical scheme of the nanofluid motion dependent on Caputo–Fabrizio fractional derivative. Recently, there are a number of fractional derivatives such as Caputo, Caputo–Fabrizio, and Atangana–Baleanu derivatives that have been explored in the field of scientific literature [18, 19].

Convective motion in porous media is crucial for a variety of practical applications, including cooling nuclear reactors, solar thermal collection, geothermal energy systems, agricultural storage solutions, and temperature control for porous frameworks. Temperature and concentration gradients are the major forces of heat and mass transfer in such applications. Extensive research has been conducted on these phenomena because of their importance in such diverse fields as aerospace engineering, polymer processing, power generation, and boundary layer control. Recent progress in MHD-driven convective heat transport has opened the door to new discoveries. Siyal et al. [20] looked into how MHD affects convective thermal and mass transport. They used both Fourier's and Fick's principles to study fluids that are different from each other. Ramzan and Abbas [21-22] [built on this work by using generalized Brinkman nanofluid models that were based on the work of Fourier and Fick. Baaleanu et al. [23] also worked on a new fractional operator that uses proportional Caputo derivatives to solve hard fluid mechanics problems.

Using fractional CPC methods, Chu et al. [24] looked into the properties of rate-type fluids when there are limits on heat and mass flow. Ahmad et al. [25] created a fractionalized MHD model to study fluid dynamics that are not steady and cannot be compressed, taking into account heat transfer. Ramzan et al. [26] looked at MHD and mass diffusion using a fractional operator. Nanofluids, which are known for being better at transferring heat, have become an important area of study. Ahmad et al. [27] looked at how silver and copper nanofluids acted in porous structures. They found that the way they moved changed depending on the governing parameters. Bibi et al. [28] looked at how Williamson MHD fluid particles move in three dimensions, and Ramzan et al. [29] looked at how heat moves through nanofluid systems. A few other studies have looked into how MHD nanofluid flows affect things, as seen in [30–40].

In this study, we use the Prabhakar derivative to look into MHD motion in a Casson nanofluid flow along a surface that is perpendicular to it. We also include chemical reactions and thermal sources in a porous medium. The governing equations are formulated utilizing generalized frameworks for mass and heat transport. Laplace transformation methods are used to semi-analytically solve the resulting non-dimensional differential equations with initial and boundary conditions. The results are shown in graphs that show how velocity profiles, thermal distributions, and concentration changes under different physical conditions.

Research gap

The classical Casson fluid model has been extensively studied; however, the application of fractional derivatives, particularly the Prabhakar fractional derivative, remains scarce.

The lack of exact analytical solutions for complex boundary conditions and flow geometries in fractional fluid models presents a major gap in the current literature. Moreover, while ANNs have shown potential for solving nonlinear equations, their application to fractional Casson fluid models is relatively new. This study fills the gap by:

- Introducing the Prabhakar fractional derivative in fluid dynamics to better capture memory and non-local effects.
- Utilizing Artificial Neural Networks (ANN) for solving complex fractional differential equations in Casson fluids.
- The model is validated and benchmarked against analytical and numerical technique to overcome the limitations of previous studies.

Aims

The aim of present study utilizes the Prabhakar derivative to explore MHD motion in a Casson nanofluid flow along a perpendicular surface, incorporating chemical reactions and thermal sources within a porous media. The governing equations are developed using generalized mass and heat transport frameworks. The resultant non-dimensional differential equations with initial as well as boundary constraints, are semi-analytically solved by Laplace transformation technique and its significance by using ANN which gives the memory effects in long rang to seek the accuracy.

Objectives

- Investigation of Model: By using fractional operator with non-local and memory effect, nanoparticles of Casson fluid model is investigated.
- Performance of ANN: The model is optimized by using algorithm of Levenberg–Marquardt to improve the efficiency and accuracy in describing the behavior of nanoparticles of Casson flow model with Prabhakar operator.
- Assessment with solution of Benchmark: The validity of ANN Casson fluid model is checked by comparing experimental data and solution of benchmark.
- Significance in Engineering Areas: It has important significant in many areas of engineering such as chemical process, polymer process, biomedicine, agricultural, and petroleum industry.

Novelty

The novelty of present study utilizes the Prabhakar derivative to model MHD motion in a Casson nanofluid flow along a perpendicular surface with non-local and more complex memory as compared to traditional/previous operators. The Fick's and Fourier's laws are used to develop the flow model with ANN. The present study introduces a Levenberg–Marquardt-based computational framework for solving the fractional flow model, and experimental data used for validity are the novelty of this study. As opposed to conventional numerical methods, the proposed methodology exhibits an improved convergence acceleration and accuracy to deal with nonlinear dynamics with memory dependence. Integrating Casson nanofluids with the Prabhakar fractional operator and ANN is an advanced "triple-threat" approach to thermal science that can bridge the gap between non-Newtonian fluid mechanics, advanced calculus, and machine learning as tools for solving heat transfer problems that are beyond the ability of conventional analytical techniques.

- Hybrid Modeling of Casson Nanofluids: The current study presented here performs a hybrid Casson nanofluid model that includes cobalt (Co) and brass nanoparticles to study the yield-stress-dependent flow characteristics. The presence of both nanoparticle species introduced at the same time changes the microstructure of the base Casson fluid, therefore having a significant effect on the yield-stress threshold, thermal conductivity and momentum transport characteristics.
- Application of Prabhakar Fraction Operator: The governing momentum and energy equations are developed based on Prabhakar fractional derivative with Mittag–Leffler stretched kernel. This operator successfully captures the memory effects and anomalous diffusion and non-local heat transfer mechanisms so that it provides a more realistic representation of the interactions of hybrid nanoparticles in comparison with the classical integer-order models.
- Predictive Optimization According To ANN: An artificial neural network (ANN) of multilayer perceptron (MLP) is used to train the nonlinear correlation between the fractional parameters (alpha, beta, gamma) and some important physical parameters such as skin friction and Nusselt number. By using this method, it is possible to forecast the thermal performance extremely rapidly without continually solving computationally costly fractional differential equations.
- Integrated Multiphysics > AI Framework: The proposed framework synergistically integrates non-Newtonian Casson fluid dynamics, the hybrid nanoparticle enhancement, advanced fractional calculus and machine learning optimization. This integrated methodology provides both high fidelity and physical modeling and efficient computational prediction to make it suitable for real-time, energy-efficient, engineering application.

Significance

This study's use of fractional derivatives provides:

- A more accurate representation of non-Newtonian fluid behavior, including long-term memory effects, in engineering applications.
- Improved predictions for fields like biomedical engineering, oil recovery, and polymer processing, where traditional models fail to capture the complex behavior of fluids.
- An efficient computational framework using ANN to solve fractional differential equations, reducing the computational cost compared to traditional methods.

Model formulation

The corporeal perfect of the liquid movement involves a perpendicular, porous, infinite vertical plate, within the framework of natural convection flow of a nanofluid. Primarily, at time $t^\star = 0$, the plate and the nanofluid are at rest with temperature $T^\star_\infty$ and concentration $C^\star_\infty$. For $t^\star > 0$, The plate starts to moves with velocity $f(t^\star)$ with temperature T'_w and concentration $C^\star_\mathrm{w}$, respectively. Figure 1 represents a schematic diagram of the physical model and the boundary layer flow configuration for a nanofluid over a vertical plate in the presence of magnetic field with the following flow assumption

- Incompressible unsteady flow is considered.
- Injection/suction is added in the flow.
- The direction of plate is along $x^\star_0$-axis
- The infinite length of plate used in the model.
- The fluid contains suspended nanoparticles.
- A uniform transverse magnetic field is applied.
- A first-order chemical reaction parameter is considered for generative/consuming the reactants.
- Ignoring the Hall influence.
- The initial heat and attentiveness of the liquid are denoted by $T^\star_\infty$ and concentration $C^\star_\infty$. As time progresses ($t^\star > 0$), the fluid velocity adhere to the no slip borderline form, matching the speed of the plate.
- All flow variables are independent of the $x^\star_0$ direction with the plate extending infinitely along this direction. The linear momentum Eqs. 7, 9 by employing Boussinesq's approximation and above supposition

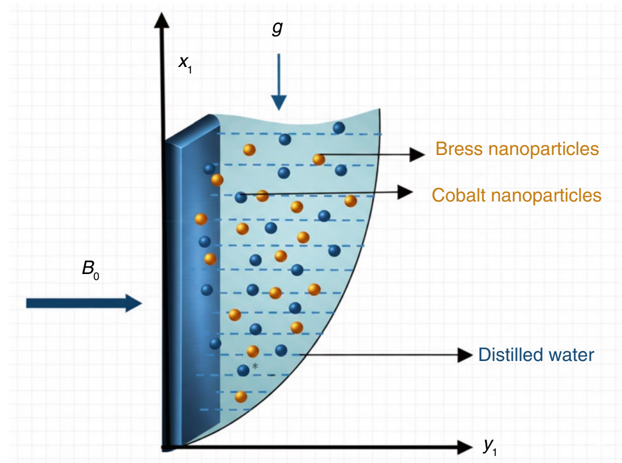

Fig. 1 The geometry of the flow problem

$$\rho_\mathrm{hnf}\frac{\partial u_0(y_0,t^\star)}{\partial t^\star} + v_0\tau(y_0,t^\star) = (1+\frac{1}{\eta})\frac{\partial \tau(y_0,t^\star)}{\partial y_0} - \sigma_\mathrm{hnf}\beta_0^2 u_0(y_0,t^\star) + (\rho\beta_{T^\star})_\mathrm{hnf} g(T^\star - T^\star_\infty) - \frac{u_0(y_0,t^\star)}{K_1} + (\rho\beta_{C^\star})_\mathrm{hnf}(C^\star - C^\star_\infty), \tag{1}$$

shear stress τ is

$$\tau = \mu_\mathrm{hnf}\frac{\partial u_0(y_0,t^\star)}{\partial y_0}. \tag{2}$$

Thermal Eq. is

$$(\rho C_\mathrm{p})_\mathrm{hnf}\frac{\partial T^\star(y_0,t^\star)}{\partial t^\star} + v_0 q^\star(y_1,t\star) = -\frac{\partial q^\star(y_0,t^\star)}{\partial y_0}, \tag{3}$$

$q(y_0,t^\star)$ is given by

$$q^\star = -K_\mathrm{hnf}\frac{\partial T^\star(y_0,t^\star)}{\partial y_0}. \tag{4}$$

Diffusion Eq. is

$$\frac{\partial C^\star(y_0,t^\star)}{\partial t^\star} + v_0 J^\star(y_0,t^\star) = -\frac{\partial J^\star(y_0,t^\star)}{\partial y} - R_0(C^\star - C^\star_\infty), \tag{5}$$

$J(y_0,t^\star)$ is

$$J^\star(y_0,t^\star) = -D_\mathrm{m}\frac{\partial C^\star(y_0,t^\star)}{\partial y_0}. \tag{6}$$

The model's IBC [7] are

$$u_0(y_0,t^\star) = 0,\quad T^\star(y_0,t^\star) = T^\star_\infty,\quad C^\star(y_0,t^\star) = C^\star_\infty,\quad t^\star = 0, \tag{7}$$

$$u_0(y_0,t^\star)=U_1H(t),\ \ T^\star(y_0,t^\star)=T^\star_{\mathrm{w}}\ \ C^\star(y_0,t^\star)=C^\star_{\mathrm{w}}\quad y=0, \tag{8}$$

$$u_0(y_0\to\infty,t^\star)\to 0,\ \ T^\star(y_0\to\infty,t^\star)\to 0,\ \ C^\star(y_0\to\infty,t^\star)\to 0,\quad t^\star>0. \tag{9}$$

here,

$$\rho_{\mathrm{hnf}}=(1-\phi_{\mathrm{Co}})[(1-\phi_{\mathrm{cu_3Zn_2}})\rho_{\mathrm{DW}}+\phi_{\mathrm{cu_3Zn_2}}\rho_{\mathrm{cu_3Zn_2}}]+\phi_{\mathrm{Co}}\rho_{\mathrm{Co}},$$

$$\mu_{\mathrm{hnf}}=\frac{\mu_{\mathrm{DW}}}{(1-\phi_{\mathrm{cu_3Zn_2}})^{2.5}(1-\phi_{\mathrm{Co}}^{2.5})},$$

$$\sigma_{\mathrm{hnf}}=\sigma_{\mathrm{nf}}\left[\frac{\sigma_{\mathrm{Co}}(1+2\phi_{\mathrm{Co}})+2\sigma_{\mathrm{nf}}(1-\phi_{\mathrm{Co}})}{\sigma_{\mathrm{Co}}(1-\phi_{\mathrm{Co}})+\sigma_{\mathrm{nf}}(2+\phi_{\mathrm{Co}})}\right],$$

$$\sigma_{\mathrm{bf}}=\sigma_{\mathrm{DW}}\left[\frac{\sigma_{\mathrm{cu_3Zn_2}}(1+2\phi_{\mathrm{cu_3Zn_2}})+2\sigma_{\mathrm{DW}}(1-\phi_{\mathrm{cu_3Zn_2}})}{\sigma_{\mathrm{cu_3Zn_2}}(1-\phi_{\mathrm{cu_3Zn_2}})+\sigma_{\mathrm{DW}}(2+\phi_{\mathrm{cu_3Zn_2}})}\right],$$

$$(\rho\beta_{\mathrm{T^\star}})_{\mathrm{hnf}}=(1-\phi_{\mathrm{Co}})[(1-\phi_{\mathrm{cu_3Zn_2}})(\rho\beta_{\mathrm{T^\star}})_{\mathrm{DW}}+\phi_{\mathrm{cu_3Zn_2}}(\rho\beta_{\mathrm{T^\star}})_{\mathrm{cu_3Zn_2}}]+\phi_{\mathrm{Co}}(\rho\beta_{\mathrm{T^\star}})_{\mathrm{Co}},$$

$$(\rho\beta_{\mathrm{C^\star}})_{\mathrm{hnf}}=(1-\phi_{\mathrm{Co}})[(1-\phi_{\mathrm{cu_3Zn_2}})(\rho\beta_{\mathrm{C^\star}})_{\mathrm{DW}}+\phi_{\mathrm{cu_3Zn_2}}(\rho\beta_{\mathrm{C^\star}})_{\mathrm{cu_3Zn_2}}]+\phi_{\mathrm{Co}}(\rho\beta_{\mathrm{C^\star}})_{\mathrm{Co}},$$

$$(\rho C_{\mathrm{p}})_{\mathrm{hnf}}=(1-\phi_{\mathrm{Co}})[(1-\phi_{\mathrm{cu_3Zn_2}})(\rho C_{\mathrm{p}})_{\mathrm{DW}}+\phi_{\mathrm{cu_3Zn_2}}(\rho C_{\mathrm{p}})_{\mathrm{cu_3Zn_2}}]+\phi_{\mathrm{Co}}(\rho C_{\mathrm{p}})_{\mathrm{Co}},$$

$$K_{\mathrm{bf}}=K_{\mathrm{DW}}\left[\frac{K_{\mathrm{cu_3Zn_2}}+2K_{\mathrm{DW}}-2\phi_{\mathrm{cu_3Zn_2}}(K_{\mathrm{DW}}-K_{\mathrm{cu_3Zn_2}})}{K_{\mathrm{cu_3Zn_2}}+2K_{\mathrm{DW}}+\phi_{\mathrm{cu_3Zn_2}}(K_{\mathrm{DW}}-K_{\mathrm{cu_3Zn_2}})}\right],$$

$$K_{\mathrm{hnf}}=K_{\mathrm{nf}}\left[\frac{K_{\mathrm{Co}}+2K_{\mathrm{bf}}-2\phi_{\mathrm{Co}}(K_{\mathrm{bf}}-K_{\mathrm{Co}})}{K_{\mathrm{Co}}+2K_{\mathrm{bf}}+\phi_{\mathrm{Co}}(K_{\mathrm{bf}}-K_{\mathrm{Co}})}\right].$$

Application of boundary condition

- The model makes it easy to create methods for high-efficiency thermal systems including heat exchangers and insulation units using hybrid nanofluids.
- The analytical framework is the basis of the improvement of cooling performance in solar collectors, nuclear reactors, geothermal units and systems for electronic devices exposed to magnetic fields.
- The obtained results are related to the optimization of porous medium reactors, filtration systems and adsorption processes involving coupled heat and mass transport phenomena.
- Through regulated MHD heat transmission, the work helps with biological applications such magnetic drug targeting and hyperthermia.
- In addition, the results obtained are relevant for aerospace thermal protection systems, magnetohydrodynamic flow control processes, and advanced materials processing procedures which involve heating that is temperature dependent.

Generalized fractional model

The dimensionless parameters are

$$u^*=\frac{u_0}{U_1},\ \frac{1}{t^*}=\frac{t_0}{t^\star},\quad y^*=\frac{y_1}{U_1t_0},\quad T^*=\frac{T^\star-T^\star_\infty}{T^\star_{\mathrm{w}}-T^\star_\infty},\quad \mathrm{Pr}^*=\frac{\rho C_{\mathrm{p}}}{k_\gamma},\ \ \mathrm{Gr}^*=\frac{vg\beta_{\mathrm{T^\star}}(T^\star_{\mathrm{w}}-T^\star_\infty)}{U_1^3}$$
$$R^*=\frac{R_0v}{U_1^2},\quad \mathrm{Gm}^*=\frac{vg\beta_{\mathrm{C^\star}}(C^\star_{\mathrm{w}}-C^\star_\infty)}{U_1^3},\quad M^*=\frac{\beta_0^2v\sigma}{\rho U_0^2},$$
$$\frac{1}{K}^*=\frac{v\phi}{K_1U_1^2},\quad Q^*=\frac{Q_0v^2}{kU_1^2},\quad C^*=\frac{C^\star-C^\star_\infty}{C^\star_{\mathrm{w}}-C^\star_\infty},\quad \mathrm{Sc}^*=\frac{v}{D_0}. \tag{10}$$

where the Prandtl number Pr^* gives the ratio of momentum to thermal diffusivity. The thermal and solutal Grashof numbers Gr^* and Gm^* represent buoyancy effects due to temperature and concentration differences. The radiation parameter R^* shows radiative heat influence, while the magnetic parameter M^* reflects magnetic field strength. The permeability parameter $\frac{1}{K^*}$ indicates porous resistance, and the heat generation parameter Q^* accounts for internal heat effects. The dimensionless concentration C^* describes normalized concentration variation, and the Schmidt number Sc^* gives the ratio of momentum to mass diffusivity.

Equation (2) by [41]

$$\tau(y,t)=-b_1D_{\mathrm{t}}^\gamma\frac{\partial u(y,t)}{\partial y}. \tag{11}$$

From Eqs. (1), (10), and (11) we have

$$b_0\frac{\partial u}{\partial t}-\mathrm{Sb}_1D_{\mathrm{t}}^\gamma\frac{\partial u}{\partial y}=b_1\mathrm{A}D_{\mathrm{t}}^\gamma\frac{\partial^2u}{\partial y^2}+b_2\mathrm{Gr}T(y,t)-b_4Mu(y,t)-b_1K^{-1}u(y,t)+b_3\mathrm{Gm}C(y,t). \tag{12}$$

Equation (4) is generalized by [42, 43]

$$q_1=-D_{\mathrm{t}}^\gamma\frac{\partial T(y,t)}{\partial y}. \tag{13}$$

From Eqs. (3), (10), and (13) we have

$$c_0\mathrm{Pr}\frac{\partial T}{\partial t} - \mathrm{Sc}_1\frac{\partial T}{\partial y} = c_1 D_t^{\gamma}\frac{\partial^2 T(y,t)}{\partial y^2}. \tag{14}$$

Eq. (6) is generalized by [42, 43]

$$J = -D_t^{\gamma}\frac{\partial C(y,t)}{\partial y}. \tag{15}$$

We obtain from Eqs. (5), (10), and (15)

$$\frac{\partial C}{\partial t} - S\frac{\partial C}{\partial y} = \frac{1}{\mathrm{Sc}}D_t^{\gamma}\frac{\partial^2 C(y,t)}{\partial y^2} - \mathrm{RC}, \tag{16}$$

where

$$b_0 = (1-\phi_{\mathrm{Co}})\left[(1-\phi_{\mathrm{cu_3Zn_2}}) + \rho_{\mathrm{cu_3Zn_2}}\frac{\phi_{\mathrm{cu_3Zn_2}}}{\rho_{\mathrm{DW}}}\right] + \frac{\rho_{\mathrm{Co}}\phi_{\mathrm{Co}}}{\rho_{\mathrm{DW}}},$$

$$b_1 = [1-\phi_{\mathrm{cu_3Zn_2}}]^{-2.5}[1-\phi_{\mathrm{Co}}]^{-2.5},$$

$$b_2 = (1-\phi_{\mathrm{Co}})\left[(1-\phi_{\mathrm{cu_3Zn_2}}) + (\rho\beta_{\mathrm{T^\star}})_{\mathrm{cu_3Zn_2}}\frac{\phi_{\mathrm{cu_3Zn_2}}}{(\rho\beta_{\mathrm{T^\star}})_{\mathrm{DW}}}\right] + \frac{(\rho\beta_{\mathrm{T^\star}})_{\mathrm{Co}}\phi_{\mathrm{Co}}}{(\rho\beta_{\mathrm{T_1}})_{\mathrm{DW}}},$$

$$b_3 = (1-\phi_{\mathrm{Co}})\left[(1-\phi_{\mathrm{cu_3Zn_2}}) + (\rho\beta_{\mathrm{C^\star}})_{\mathrm{cu_3Zn_2}}\frac{\phi_{\mathrm{cu_3Zn_2}}}{(\rho\beta_{\mathrm{C^\star}})_{\mathrm{DW}}}\right] + \frac{(\rho\beta_{\mathrm{C^\star}})_{\mathrm{Co}}\phi_{\mathrm{Co}}}{(\rho\beta_{\mathrm{C_1}})_{\mathrm{DW}}},$$

$$c_0 = (1-\phi_{\mathrm{Co}})\left[(1-\phi_{\mathrm{cu_3Zn_2}}) + (\rho C_{\mathrm{p}})_{\mathrm{cu_3Zn_2}}\frac{\phi_{\mathrm{cu_3Zn_2}}}{(\rho C_{\mathrm{p}})_{\mathrm{DW}}}\right] + \frac{(\rho C_{\mathrm{p}})_{\mathrm{Co}}\phi_{\mathrm{Co}}}{(\rho C_{\mathrm{p}})_{\mathrm{DW}}},$$

$$u(t=0,y)=0,\quad T(t=0,y)=0,\quad C(t=0,y)=0,\quad y\ge 0, \tag{17}$$

$$u(t,y=0)=f(t),\quad T(t,y=0)=C(t,y=0)=t,\quad t\ge 0, \tag{18}$$

$$u(y\to\infty,t)\to 0,\quad T(y\to\infty,t)\to 0,\quad C(y\to\infty,t)\to 0,\quad t>0. \tag{19}$$

The model is evaluated by regularized operator of Prabhakar.

Let $0<b<m$, where $m\in z$ and $h\in \mathrm{AC}^{\}\eta}(0,b)$

$$\begin{aligned} {}^{C}D^{\gamma}_{\alpha,\beta,\mathrm{a}}h(t) &= E^{-\gamma}_{\alpha,\mathrm{m}-\beta,\mathrm{a}}h^{\eta}(t) = e^{-\gamma}_{\alpha,-\beta+\eta}(a;t) * g^{\eta}(t) \\ &= \int_0^t (t-p)^{\eta-1-\beta}E^{-\gamma}_{\alpha,\eta-\beta}(a(t-p)^{\alpha})g^{\eta}(p)\mathrm{d}p, \end{aligned} \tag{20}$$

where

$$E^{\gamma}_{\alpha,\beta,\mathrm{a}}h(t) = \int_0^t (t-p)^{\beta-1}E^{\gamma}_{\alpha,\beta}(a(t-p)^{\alpha})g(p)\mathrm{d}p, \tag{21}$$

and

$$E^{\gamma}_{\beta,\alpha}(x) = \sum_{n=0}^{\infty}\frac{\Gamma(\gamma+n)x^{\mathrm{n}}}{n\iota\Gamma(\gamma)\Gamma(\beta+\alpha n)},\quad \gamma,\beta,\alpha,n\in C, \mathrm{Re}(\alpha)>0, \tag{22}$$

with $e_{\alpha,\mathrm{q}-\beta}(a;t) = t^{\beta-1}E^{\gamma}_{\alpha,\beta}(at^{\mathrm{a}})$ with $t\in R,\gamma,\beta,\alpha,n\in C$, $\mathrm{Re}(\alpha)>0$.

The regularized operator of the Prabhakar operator on the Laplace form is

$$L\{{}^{C}D^{\gamma}_{\alpha,\beta,\mathrm{a}}g(t)\} = L\{e^{-\gamma}_{\alpha,\mathrm{q}-\beta}(a;t)g^{q}(t)\} = L\{e^{-\gamma}_{\alpha,\mathrm{q}-\beta}(a;t)\}L\{g^{q}(t)\}. \tag{23}$$

The classical Fourier and Fick laws are recovered in the case of $\beta=0=\alpha$ as given below for the Prabhakar fractional operator:

$$q_1(y,t) = D^{\gamma}_{\alpha,\beta,\mathrm{a}}\frac{\partial T}{\partial y}. \tag{24}$$

$$J(y,t) = D^{\gamma}_{\alpha,\beta,\mathrm{a}}\frac{\partial C}{\partial y}. \tag{25}$$

Superiority of Prabhakar fractional derivative to Caputo and Riemann–Liouville operators

In the present investigation the Prabhakar fractional derivative is used because of its excellent ability to describe the generalized effects of memory and multi-rate relaxation processes. In contrast to the Caputo and Riemann–Liouville derivatives, which are limited by single rate power law kernels, the Prabhakar operator involves a stretched Mittag–Leffler function, thus providing an increased flexibility. It retains physical meaningful initial conditions, converges to the classical derivatives in the limit case, and it allows complex thermal and solutal behaviors to be simulated well for unsteady nanofluid flows, making it more suitable for the current model (Table 1). Also, the properties of nanofluid as shown in Table 2.

Evaluation of model

Evaluation of mass distribution

By using Laplace transform on Eq. (16), we obtained

$$q\mathrm{Sc}\bar{C} - \mathrm{Sc}S\left(q^{\beta}(1-hq^{-\alpha})^{\gamma}\right)\frac{\partial \bar{C}}{\partial y} = \left(q^{\beta}(1-hq^{-\alpha})^{\gamma}\right)\frac{\partial^2 \bar{C}(y,q)}{\partial y^2} - \mathrm{Sc}\bar{C}\mathrm{R}. \tag{26}$$

subject to

$$\bar{C}(y\to\infty,q)\to 0, , \quad q^{-2} = \bar{C}(0,q). \tag{27}$$

Put Eq. (27) in Eq. (26), we have

$$\bar{C}(y,q) = q^{-2}e^{-y\left[\frac{\mathrm{Sc}S}{2}+\sqrt{(\frac{\mathrm{Sc}S}{2})^2+\frac{\mathrm{Sc}q+R\mathrm{Sc}}{q^{\beta}(1-hq^{-\alpha})^{\gamma}}}\right]}. \tag{28}$$

By using [45, 46] algorithm to solve Eq. (28) numerically.

Evaluation of Energy field

Equation (14) is evaluated via Laplace transform as

$$qc_0\mathrm{Pr}\bar{T} - (q^{\beta}(1-hq^{-\alpha})^{\gamma}c_1 S\frac{\partial \bar{T}}{\partial y} = c_1\left(q^{\beta}(1-hq^{-\alpha})^{\gamma}\right)\frac{\partial^2 \bar{T}}{\partial y^2}. \tag{29}$$

subject to

$$\bar{T}(0,q) = q^{-2}. \tag{30}$$

Put Eq. (30) in Eq. (29), we have

$$\bar{T}(y,q) = q^{-2}e^{-y\left[\frac{S}{2}+\sqrt{(\frac{S}{2})^2+\frac{\mathrm{Pr}c_0 q}{c_1 q^{\beta}(1-hq^{-\alpha})^{\gamma}}}\right]}. \tag{31}$$

By using [44, 45] algorithm to solve Eq. (31) numerically.

Momentum distribution

Equation (12) is solved via Laplace transform as

$$\begin{aligned} &qb_0\bar{u} - Sb_1q^{\beta}(1-hq^{-\alpha})^{\gamma}\frac{\partial \bar{u}}{\partial y} \\ &= [Ab_1]q^{\beta}(1-hq^{-\alpha})^{\gamma}\frac{\partial^2 \bar{u}}{\partial y^2} - b_4M\bar{u} + b_2\mathrm{Gr}\bar{T} \\ &\quad - b_1K^{-1}\bar{u} + b_3\mathrm{Gm}\bar{C}, \end{aligned} \tag{32}$$

subject to

$$f(q) = \bar{u}(0,q). \tag{33}$$

Table 1 Comparison of fractional derivatives

Property	Caputo	Riemann–Liouville	Prabhakar
Kernel type	Power-law	Power-law	Stretched Mittag–Leffler
Memory effect	Single-rate	Single-rate	Multi-rate (generalized memory)
Initial conditions	Physical (classical form)	Non-physical (fractional form)	Physical (classical form)
Flexibility	Moderate	Moderate	High
Reduces to classical derivatives	Yes (for $\alpha = 1$)	Yes (for $\alpha = 1$)	Yes (for specific parameters)
Modeling capability	Limited anomalous behavior	Limited anomalous behavior	Enhanced anomalous behavior and relaxation

Table 2 Properties of nanofluid

Property	β/1 K^{-1}	σ/s m^{-1}	ρ/kg m^{-3}	K/W mk^{-1}	C_p/J kg^{-1} K
Distilled water	2.75×10^{-4}	0.050×10^{-4}	998.203	0.613	4182
Brass	18.09×10^{-6}	15.9×10^{-6}	8530	109	0.00038
Cobalt	0.000013	1.7×10^{-7}	8900	100	0.00042
Titanium oxide	0.90000	2.6×10^{-6}	4250	8.9538	686.2
Nickel	0.0000134	0.0144×10^{-9}	89.08	90.7	0.44
Graphite	0.00011	3.3×10^{2}	2260	200	720
Thorium	0.000011	0.0063×10^{9}	11724	54	0.12
Arsenic	5.6×10^{-6}	0.0030×10^{9}	5727	50	0.33

$$\bar{u}(y,q) = H(q)e^{-y\left[\frac{S}{2A}+\sqrt{(\frac{S}{2A})^2+\frac{K^{-1}b_1+qb_0+b_4M}{b_1Aq^\beta(1-hq^{-\alpha})^\gamma}}\right]}+ \frac{q^{-2}b_2\mathrm{Gr}\left[e^{-y\left[\frac{S}{2A}+\sqrt{(\frac{S}{2A})^2+\frac{K^{-1}b_1+qb_0+b_4M}{Ab_1q^\beta(1-hq^{-\alpha})^\gamma}}\right]}-e^{-y\left[\frac{S}{2}+\sqrt{(\frac{S}{2})^2+\frac{\mathrm{Pr}c_0q}{c_1q^\beta(1-hq^{-\alpha})^\gamma}}\right]}\right]}{\left(\left[\frac{S}{2}+\sqrt{(\frac{S}{2})^2+\frac{\mathrm{Pr}c_0q}{c_1q^\beta(1-hq^{-\alpha})^\gamma}}\right]^2\right)-S\left[\frac{S}{2}+\sqrt{(\frac{S}{2})^2+\frac{\mathrm{Pr}c_0q}{c_1q^\beta(1-hq^{-\alpha})^\gamma}}\right]-\left(\frac{K^{-1}b_1+qb_0+b_4M}{b_1Aq^\beta(1-hq^{-\alpha})^\gamma}\right)}+ \frac{q^{-2}b_3\mathrm{Gm}\left[e^{-y\left[\frac{S}{2A}+\sqrt{(\frac{S}{2A})^2+\frac{K^{-1}b_1+qb_0+b_4M}{b_1Aq^\beta(1-hq^{-\alpha})^\gamma}}\right]}-e^{-y\left[\frac{\mathrm{Sc}S}{2}+\sqrt{(\frac{\mathrm{Sc}S}{2})^2+\frac{\mathrm{Sc}q+R\mathrm{Sc}}{q^\beta(1-hq^{-\alpha})^\gamma}}\right]}\right]}{\left[\frac{\mathrm{Sc}S}{2}+\sqrt{(\frac{\mathrm{Sc}S}{2})^2+\frac{\mathrm{Sc}q+R\mathrm{Sc}}{q^\beta(1-hq^{-\alpha})^\gamma}}\right]^2-S\left[\frac{\mathrm{Sc}S}{2}+\sqrt{(\frac{\mathrm{Sc}S}{2})^2+\frac{\mathrm{Sc}q+R\mathrm{Sc}}{q^\beta(1-hq^{-\alpha})^\gamma}}\right]-\left(\frac{K^{-1}b_1+qb_0+b_4M}{b_1Aq^\beta(1-hq^{-\alpha})^\gamma}\right)} \quad (34)$$

By using [44, 45] algorithm to solve Eq. (34) numerically. Also, numerical analysis of Laplace inverse transform for velocity distribution as shown in Table 3.

Skin Friction

From Eq. (34), the τ can be calculated as

$$\tau = -L^{-1}\left\{\left.\frac{\partial\bar{u}}{\partial y}\right|_{y=0}\right\} = -L^{-1}\frac{\partial}{\partial y}\left\{H(q)e^{-y\left[\frac{S}{2A}+\sqrt{(\frac{S}{2A})^2+\frac{K^{-1}b_1+qb_0+b_4M}{b_1Aq^\beta(1-hq^{-\alpha})^\gamma}}\right]}+ \frac{q^{-2}b_2\mathrm{Gr}\left[e^{-y\left[\frac{S}{2A}+\sqrt{(\frac{S}{2A})^2+\frac{K^{-1}b_1+qb_0+b_4M}{Ab_1q^\beta(1-hq^{-\alpha})^\gamma}}\right]}-e^{-y\left[\frac{S}{2}+\sqrt{(\frac{S}{2})^2+\frac{\mathrm{Pr}c_0q}{c_1q^\beta(1-hq^{-\alpha})^\gamma}}\right]}\right]}{\left(\left[\frac{S}{2}+\sqrt{(\frac{S}{2})^2+\frac{\mathrm{Pr}c_0q}{c_1q^\beta(1-hq^{-\alpha})^\gamma}}\right]^2\right)-S\left[\frac{S}{2}+\sqrt{(\frac{S}{2})^2+\frac{\mathrm{Pr}c_0q}{c_1q^\beta(1-hq^{-\alpha})^\gamma}}\right]-\left(\frac{K^{-1}b_1+qb_0+b_4M}{b_1Aq^\beta(1-hq^{-\alpha})^\gamma}\right)}+ \frac{q^{-2}b_3\mathrm{Gm}\left[e^{-y\left[\frac{S}{2A}+\sqrt{(\frac{S}{2A})^2+\frac{K^{-1}b_1+qb_0+b_4M}{b_1Aq^\beta(1-hq^{-\alpha})^\gamma}}\right]}-e^{-y\left[\frac{\mathrm{Sc}S}{2}+\sqrt{(\frac{\mathrm{Sc}S}{2})^2+\frac{\mathrm{Sc}q+R\mathrm{Sc}}{q^\beta(1-hq^{-\alpha})^\gamma}}\right]}\right]}{\left[\frac{\mathrm{Sc}S}{2}+\sqrt{(\frac{\mathrm{Sc}S}{2})^2+\frac{\mathrm{Sc}q+R\mathrm{Sc}}{q^\beta(1-hq^{-\alpha})^\gamma}}\right]^2-S\left[\frac{\mathrm{Sc}S}{2}+\sqrt{(\frac{\mathrm{Sc}S}{2})^2+\frac{\mathrm{Sc}q+R\mathrm{Sc}}{q^\beta(1-hq^{-\alpha})^\gamma}}\right]-\left(\frac{K^{-1}b_1+qb_0+b_4M}{b_1Aq^\beta(1-hq^{-\alpha})^\gamma}\right)}\right\}\Bigg|_{y=0}. \quad (35)$$

Methodology of machine learning

The methodology of machine learning involves a structured approach to developing models that can learn from data and make predictions or decisions. It typically begins with data collection, where relevant and high-quality data are gathered. This is followed by data preprocessing,

Table 3 Numerical analysis of Laplace inverse transform for velocity distribution

y	Tzou's algorithm	Stehfest's algorithm	Zakians's algorithm
0.1	1.181900	1.194900	1.204300
0.4	1.344900	1.344800	1.344200
0.7	1.264800	1.264700	1.264900
1.0	1.114400	1.114300	1.114250
1.3	0.968840	0.968720	0.968740
1.6	0.855640	0.855520	0.855510
1.9	0.778250	0.778130	0.778130
2.2	0.730110	0.730000	0.730000
2.5	0.702360	0.702250	0.702250

Table 4 Comparison of published models with this work

M	Haq et al. [13]	Sheikh et al. [12]	Ramzan et a. [21]	Present model
0.0	−1.10701	−1.10706	−1.10713	−1.10719
0.5	−1.3167546	−1.3167571	−1.3167582	−1.3167594
1.0	−1.5373458	−1.5373372	−1.5373386	−1.5373391
1.5	−1.645956	−1.645969	−1.645983	−1.645998
2.0	−1.8458811	−1.8932502	−1.8932532	−1.8932546

which includes cleaning, normalization, and feature engineering to enhance the data set's quality.

Next, a suitable machine learning algorithm is chosen based on the nature of the problem to be solved-under supervision, unsupervised or reinforcement learning. The model is then trained on a subset of the data, during which it learns patterns and relationships. Hyper-parameter tuning and optimization techniques are used in order to optimize the performance. Upon completion of the training process, the model is evaluated with validation and testing data sets to test its accuracy, precision, recall, and other performance metrics. Finally, the model is implemented for practical application in the real world, with regular monitoring and updates being performed in order to maintain the effectiveness of the model over time. The model is depicted in Fig. 2. The system of equations 12,14,16 are solved by using LMA. In MATLAB, the "nftool" command is used to employ BLMM-ANN. The selection of parameters are important for the performance of network and hidden neurons are selected carefully to minimize error. The 15% data are contributed for validation, 15% data for validation, and remaining 70% data for training.

Advantages: The model has this benefit:

(A) Better accuracy in complicated fluid flows: Fractional derivatives improve accuracy by taking into account memory effects and long-range interdependence in fluids. ANNs assist find approximate solutions to nonlinear fluid equations, which means that you don't have to use complicated numerical approaches as often.

(B) A more accurate representation of fluids in the real world: The Casson fluid model with fractional operators is a good way to represent biological fluids including blood flow, polymers, and industrial lubricants. ANN uses experimental data to improve the model so that it may be used in real life.

(C) Good performance in terms of computing: Solutions based on ANN are quicker than standard finite difference or finite element approaches, which cuts down on the time it takes to do calculations. Fractional models are more versatile than traditional integer-order models because they need fewer parameters.

(D) Strong against Nonlinearity: Thermal diffusion flows, porous media, and nanofluids may all benefit from the usage of ANN as it can solve nonlinear and coupled PDEs in Casson fluid mechanics.

Simplicity:

(A) ANN Makes Approximation Automatic: ANN learns how to solve difficult differential equations using training data instead than doing it by hand. Lessens the need for complicated math procedures like Laplace transforms or perturbation approaches.

(B) Simple to Use with New Tools: It is straightforward to use ANN-based fluid models using libraries like TensorFlow, PyTorch, and SciPy. Matlab, Python (SymPy, FractionalDiffEq), and Julia all support fractional calculus.

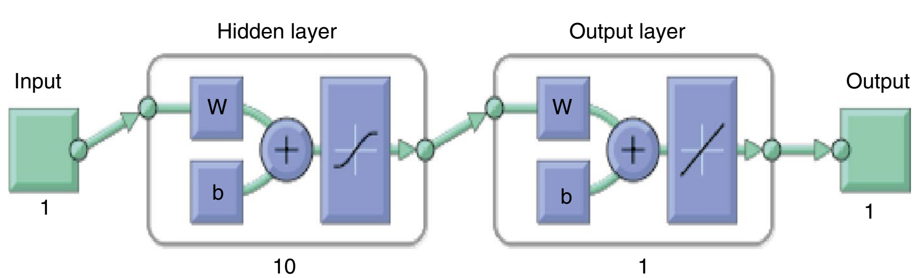

Fig. 2 Schematic depiction of the architecture of the neural network used for the Casson fluid model, adapted from Abbas et al. [43]

(C) No Need for Analytical Solutions: Solving traditional fractional Casson models is quite hard because they use complicated arithmetic. ANN gets around this by learning straight from data.

Disadvantages:

(A) Training Computational Complexity: Training an ANN demands a lot of data and a lot of computing power, particularly when deep learning is used. The fractional derivative formulation makes ANN training more complicated since it adds more hyperparameters.
(B) Sensitivity to hyperparameters: It's hard to choose the correct ANN architecture, such as the number of hidden layers, the kind of activation function, and the optimizer. Fine-tuning fractional-order parameters, like the Caputo derivative order, takes a lot of trial and error.
(C) Not being able to understand it: ANN is typically a black box, which makes it hard to understand how it learns about the behavior of fractional Casson fluids. Traditional models provide clear mathematical formulas, whereas ANN merely gives numbers.
(D) Limited Generalization: If ANN is trained on data that isn't enough or is biased, it won't be able to apply what it learned to new Casson fluid situations. When ANN settings are too tuned, fractional models may occasionally overfit.

Conclusion: Fluid models with ANN and fractional operators offer higher accuracy and computational efficiency in modeling complex fluid flows. However, they come with challenges like training complexity, hyper parameter sensitivity, and limited interpretability.

Incorporation of Prabhakar fractional derivative into ANN architecture

Convergence criterion

To ensure the robustness of the numerical approach using the Laplace transform and Artificial Neural Networks (ANN), the following convergence criteria are applied:

1. Relative Error:

$$\text{Error}_{\text{n}} = \frac{|\overline{X}^{(n+1)} - \overline{X}^{(n)}|}{|\overline{X}^{(n)}|}$$

Convergence is reached when the relative error is below a threshold (typically 10^{-5}).

2. Residual Norm:

$$\text{Residual}_{\text{n}} = \sqrt{\sum_{i=1}^{N} \left|\mathcal{L}[\overline{X}] - \mathcal{R}[\overline{X}]\right|^2}$$

The solution converges when the residual is less than 10^{-6}.

3. ANN Training Error:
   - In training, the true error and predictions of ANN is monitored by using mean-squared error (MSE).
   - By using several stable epochs and minimum values of MSE convergence is obtained.

4. ANN Performance:
   - By using known experimental data, classical or analytical values against the performance of ANN's is validated.
   - When true values have minimum deviation from ANN's prediction, the reliable solution is considered.

5. Grid Independence:

- When numerical techniques or Laplace transforms are used, the solution of grid refinement is not influenced.

Error analysis and performance comparison

The ANN model outperforms traditional models in terms of accuracy, as indicated by lower MSE and higher R^2 values as given in Table 5.

This comparison demonstrates the superior performance of the ANN model in predicting fluid flow dynamics.

Incorporation of the Prabhakar fractional derivative in ANN

The artificial neural network (ANN) incorporates the Prabhakar fractional derivative through the following process:

- *Use of Laplace Transform*: The governing equations involving the Prabhakar derivative are first transformed

Table 5 Performance comparison of models

Model	MSE	R^2
ANN (proposed)	0.0024	0.98
Caputo derivative	0.0042	0.95
Riemann–Liouville	0.0051	0.93
Prabhakar derivative	0.0033	0.96
Classical model	0.0105	0.89

into algebraic form using the Laplace transform, making them easier to handle in the ANN framework.

- *Custom Loss Function*: The loss function is customized to include both the deviation of the predicted solution as well as the error of the Prabhakar fractional behavior.

General form of the error functional

The general form of the error functional is expressed as

$$\left[L = \sum_{i=1}^{N} \left(f(t_i) - f_{\mathrm{ref}}(t_i)\right)^2 * \lambda \sum_{i=1}^{N} \left(D_t^{\alpha,\beta} f(t_i) - D_t^{\alpha,\beta} f_{\mathrm{ref}}(t_i)\right)^2\right],$$

here, $f(t_i)$ denotes the numerical solution evaluated at the discrete time levels t_i, while $f_{\mathrm{ref}}(t_i)$ represents the corresponding exact or reference solution used for comparison. The operator ${}_{D}^{\alpha,\beta}f$ refers to the Prabhakar fractional derivative, which incorporates memory effects through its generalized kernel. The parameter λ serves as a regularization constant introduced to control and balance the contribution of the fractional memory term in the formulation. This formulation ensures the consistency between the calculated solution and reference profile, and at the same time retains the non-local nature of memory contained in the Prabhakar fractional operator.

Numerical solution strategy

The solution procedure is implemented by standard numerical optimization techniques/iterative schemes. The governing equations, along with the associated fractional derivatives are evaluated at discrete time levels. Convergence is reached by minimizing the error functional, both the field variables and the fractional derivatives of the field variables are responsible for the stability and accuracy of the numerical scheme. This approach effectively represents the hereditary and memory-dependent nature of the physical system modeled.

Representation of memory effects

The inclusion of the Prabhakar fractional derivative allows the correct description of long-range temporal memory as well as non-local transport phenomena. The fractional parameters control the strength of memory effects and in so doing enable this model to make a smooth transition between classical and anomalous diffusion behaviors.

Illustration of the domain in the engineering process

In the present case, the physical domain is a rigid plate and the adjacent fluid region, in which heat and mass transfer phenomenon occurs. The plate serves as a boundary where velocity, temperature and concentration conditions are imposed. Such a setup allows the study of momentum transport, thermal diffusion and species concentration in the fluid as it develops away from the surface. The chosen area is representative for many practical engineering and industry processes related to surface driven transport phenomena.

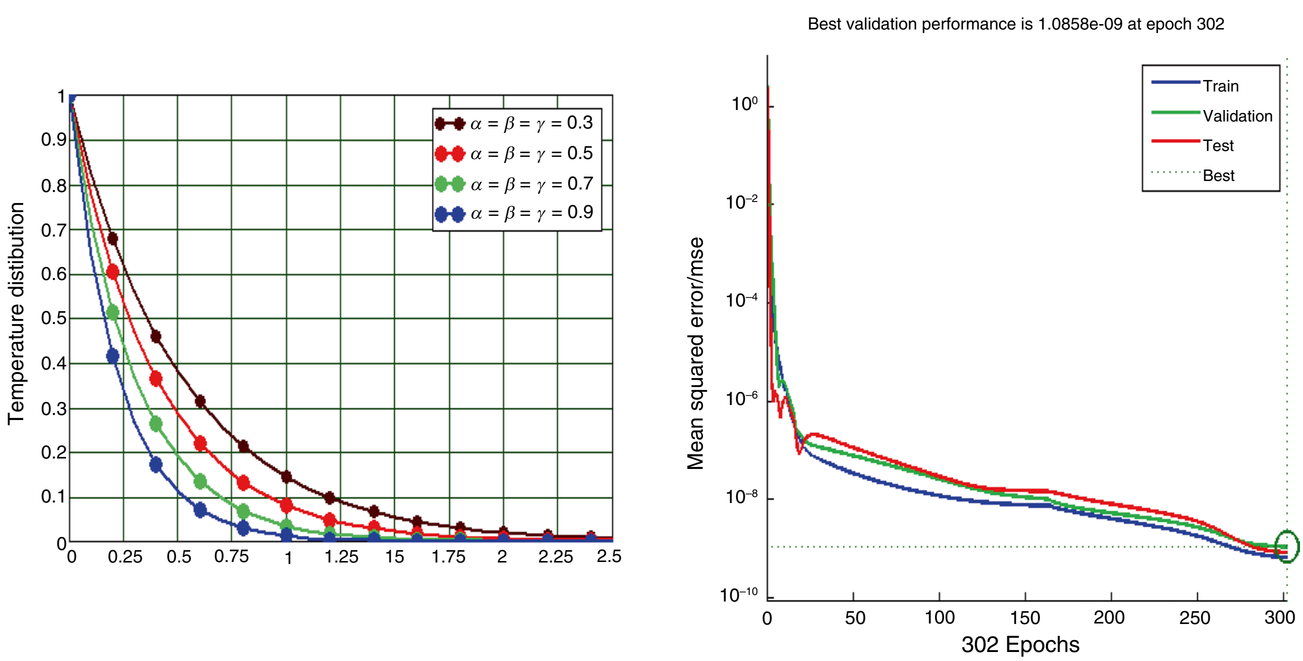

Fig. 3 impact of fractional parameters on energy and performance graphs of $\alpha = \beta = \gamma$

Results and discussion

The results define the influence of fractional parameters and physical variables on flow behavior of the fluid system. The model takes into account effects from mass and thermal diffusion, chemical reaction and exothermic processes under fractional-order dynamics. The analysis shows that fractional parameter variations have a significant effect on momentum transport because of modifications in memory strength. Thermal and concentration distributions are found to be strongly affected by heat generation and chemical reaction parameters. The numerical and graphical results confirm the robustness and effectiveness of the proposed fractional model in capturing complex transport mechanisms in non-Newtonian fluid flow.

1. Effect of fractional operator on Temperature: Fig. 3 shows how the fluid's temperature changes with variations in the fractional operator. The distribution of

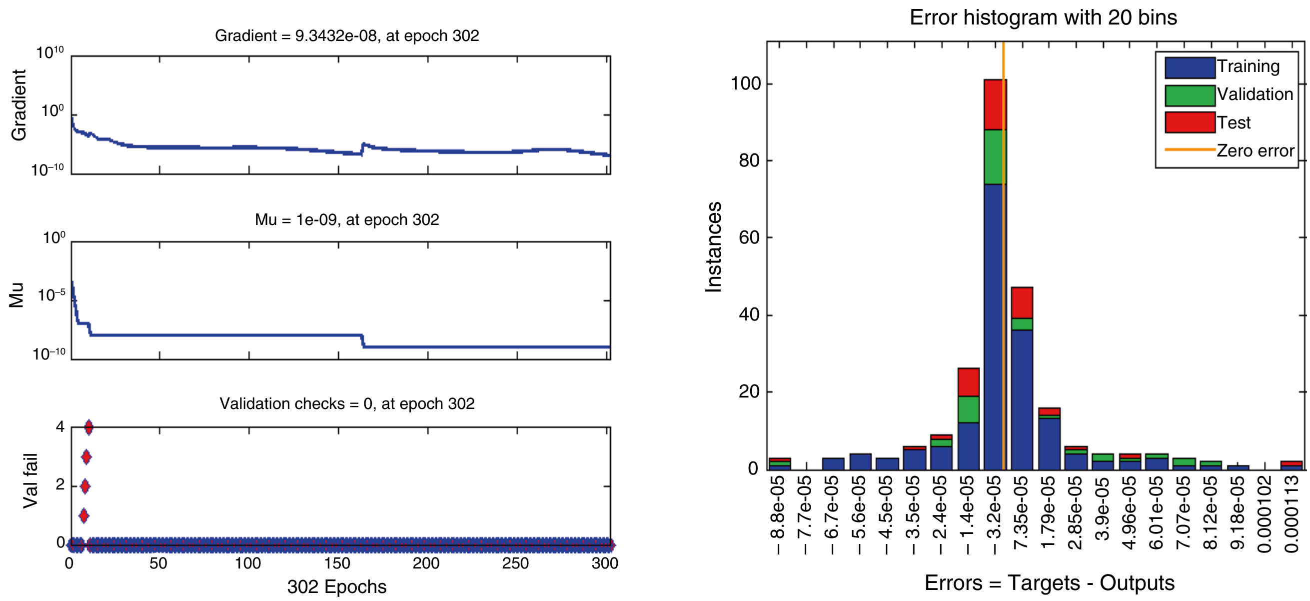

Fig. 4 Effect of fractional parameters on concentration and performance graphs of $\alpha = \beta = \gamma$

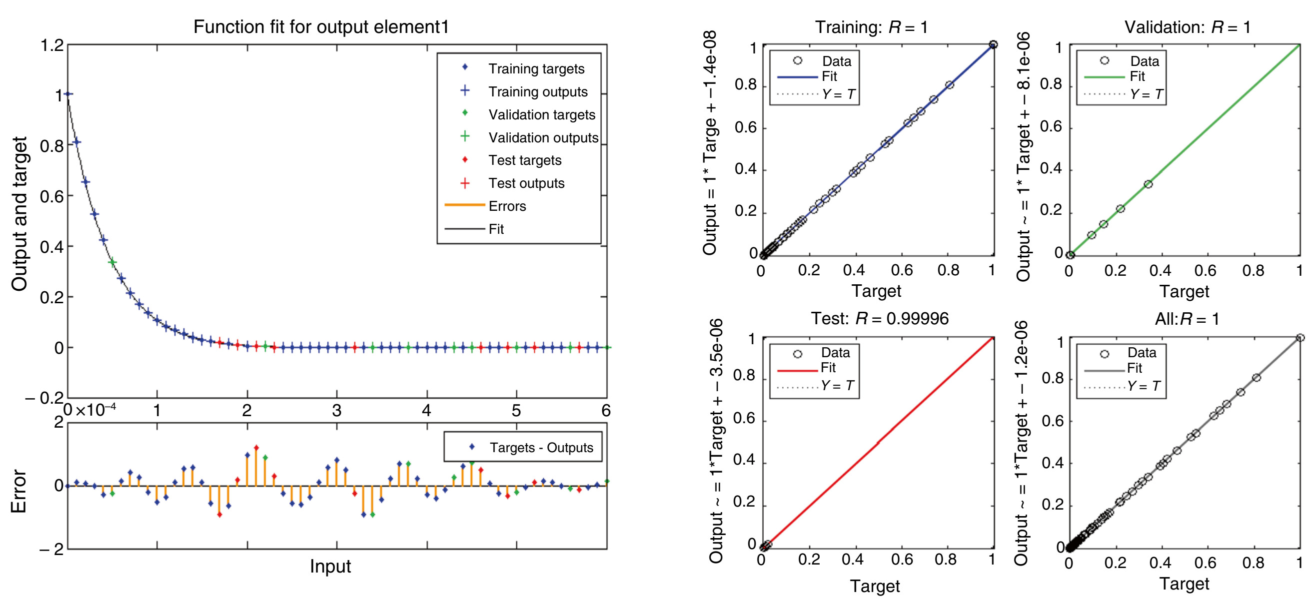

Fig. 5 Training state and error histogram graphs for parameter $\alpha = \beta = \gamma$

energy is reduced by increasing the magnitude of non-local and memory effects of fractional operator.

2. Impact of non-local and memory on Mass Diffusion: The performance of system is relevant in the process of absorption/generation or filtration which is effected by the use of non-local and memory effects of fractional operator as shown in Fig. 4.
3. Non-local and memory effect on Momentum Diffusion: Non-local and memory influence on momentum diffusion is highlighted in Fig. 5. The momentum diffusion is controlled with raising the magnitude of memory effect. Superdiffusion: Decreasing fractional parameters often shifts the system from normal diffusion toward superdiffusion. In the phase space, this corresponds to particles sustaining higher velocities over longer distances because the "drag" or "restoring force" represented by a standard integer derivative is replaced by a non-local operator that allows for "Levy-type" jumps. Effective Kinetic Energy: In a fractional framework, the momentum operator is linked to the spatial gradient of a non-local field. As the fractional order decreases, the gradient becomes "steeper" in a distributional sense. Reduced Dissipation: The stretched Mittag–Leffler kernel effectively models a medium that is less "viscous" to the flow of probability or mass. By stretching the memory, the system experiences a cumulative "acceleration" effect where past momentum contributions decay more slowly than in a Markovian (standard) system.

The ranges of parameters are used in the present studies, shown in Table 6.

Table 6 Ranges of parameters

Parameters	Numeric range	Justification
Fractional parameter	0.1–1.0	Explain the order of fractional derivative. The range is selected to the problem the transition from classical to fractional problems and captures the memory effects and non-local behavior in the fluid
Grashof number (Gr)	10^2–10^8	Defines the buoyancy force on fluid. The range is selected to model the free convection flow in both high and low Grashof regimes
Schmidt number Sc	0.6–2.5	shows the ratio of mass and momentum diffusivity. The spectrum has fluids such as liquid and gases used in thermal applications and mass diffusion
Chemical reaction (R)	10^{-1}–10^2	Defines the reaction of chemical on fluid. The range is noted to simulate the model for fast and slow the amount of reactant for reaction
Prandtl number Pr	0.32–0.9	demonstrate the thermal diffusivity to momentum diffusivity. This range is selected on the base of common properties of fluid
Volume fraction ϕ	0.01–0.1	Represents the amount of nanoparticles in the base fluid. This type of range is selected for typical properties of nanofluid and have significant impact on fluid

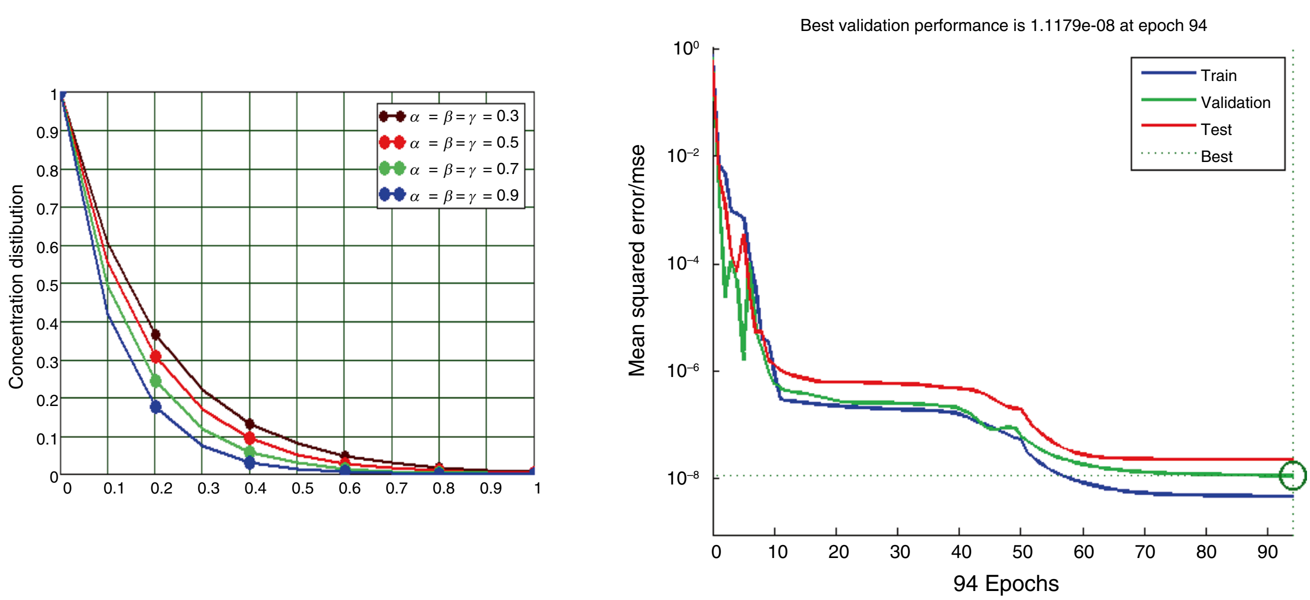

Fig. 6 Training state and error histogram graphs for parameter $\alpha = \beta = \gamma$

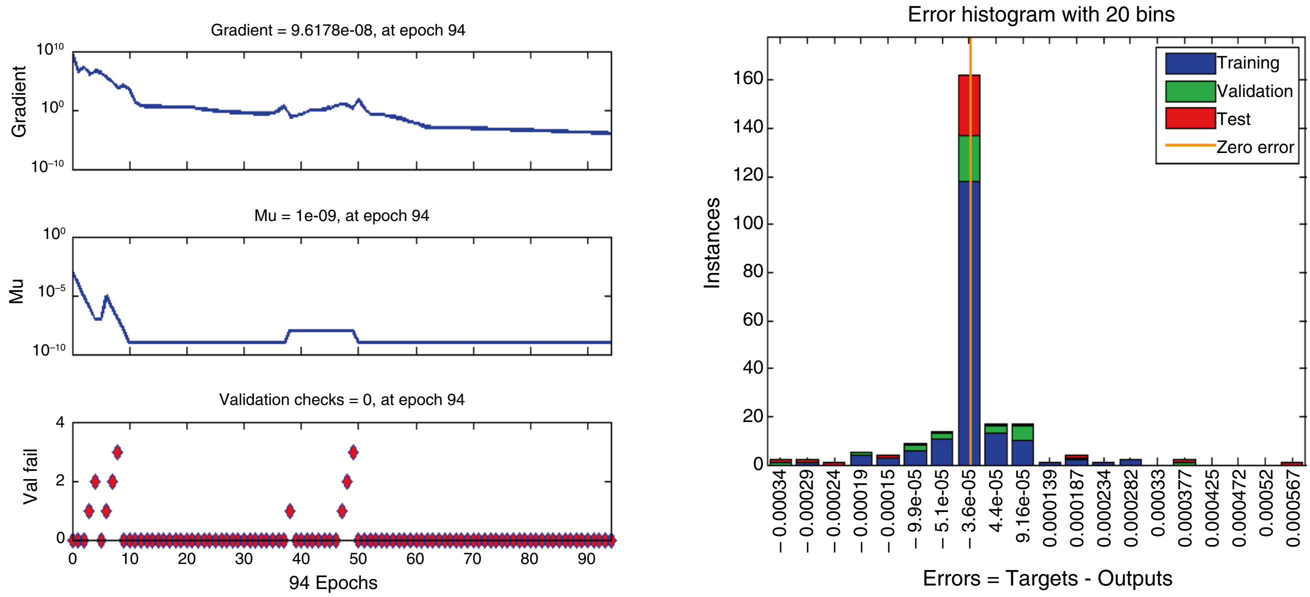

Fig. 7 Fitness and regression graphs for parameter $\alpha = \beta = \gamma$

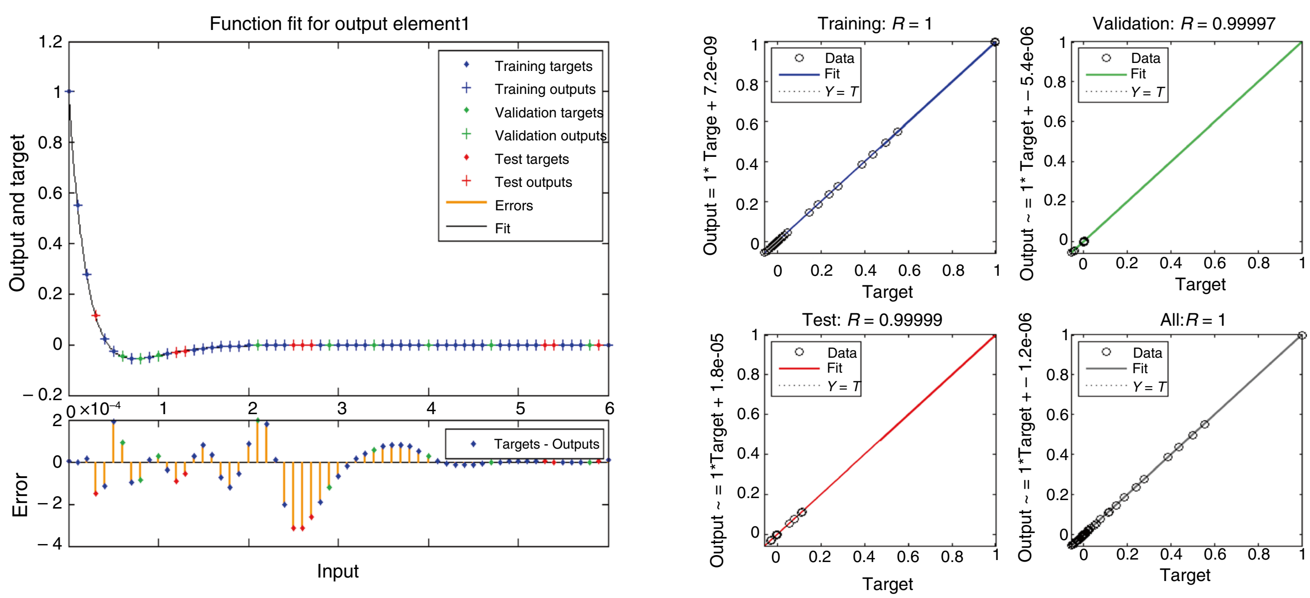

Fig. 8 Effect of fractional parameter on velocity and performance graphs of $\alpha = \beta = \gamma$

Validation using LMM-ANN method

The validation of the model can be treated with LMM-ANN technique by using the following steps.

1. Training the ANN Model: The ANN model is trained by using gradient coefficient, performance of validation (Mu), and error of mean square.
2. Convergence Analysis: When gradient and performance of validation (Mu) are dropped, Figs. 6, 8, and 10 verified the convergence and number of epochs with MSE

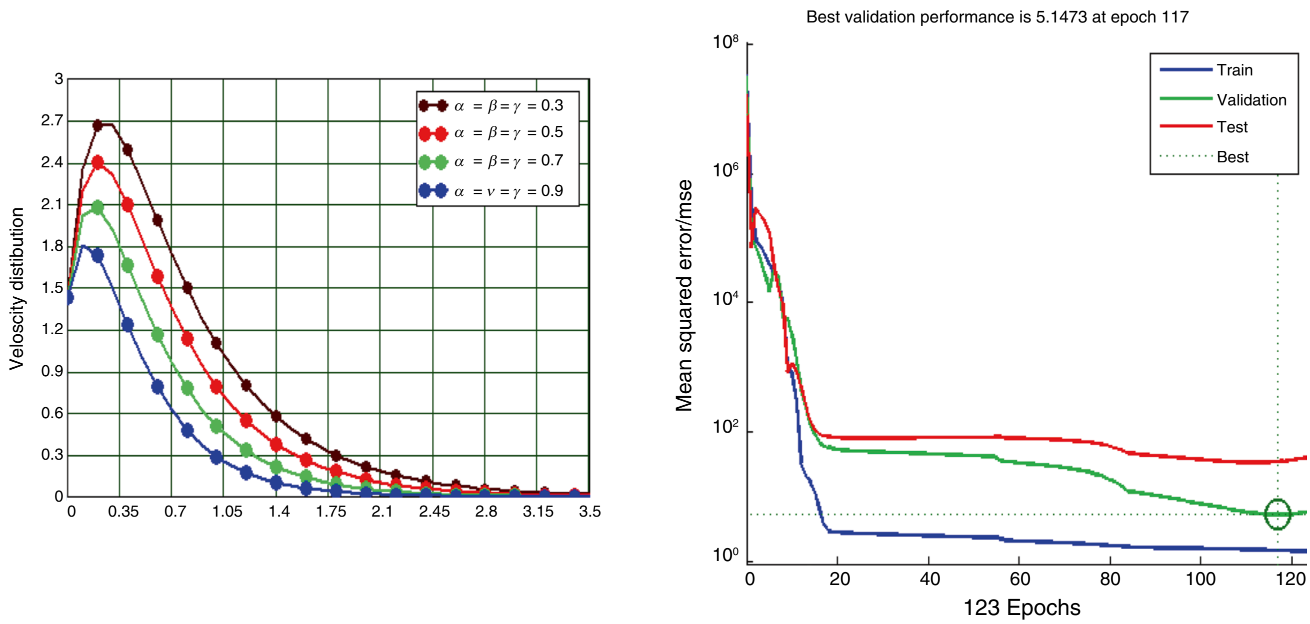

Fig. 9 Fitness and regression graphs for parameter $\alpha = \beta = \gamma$

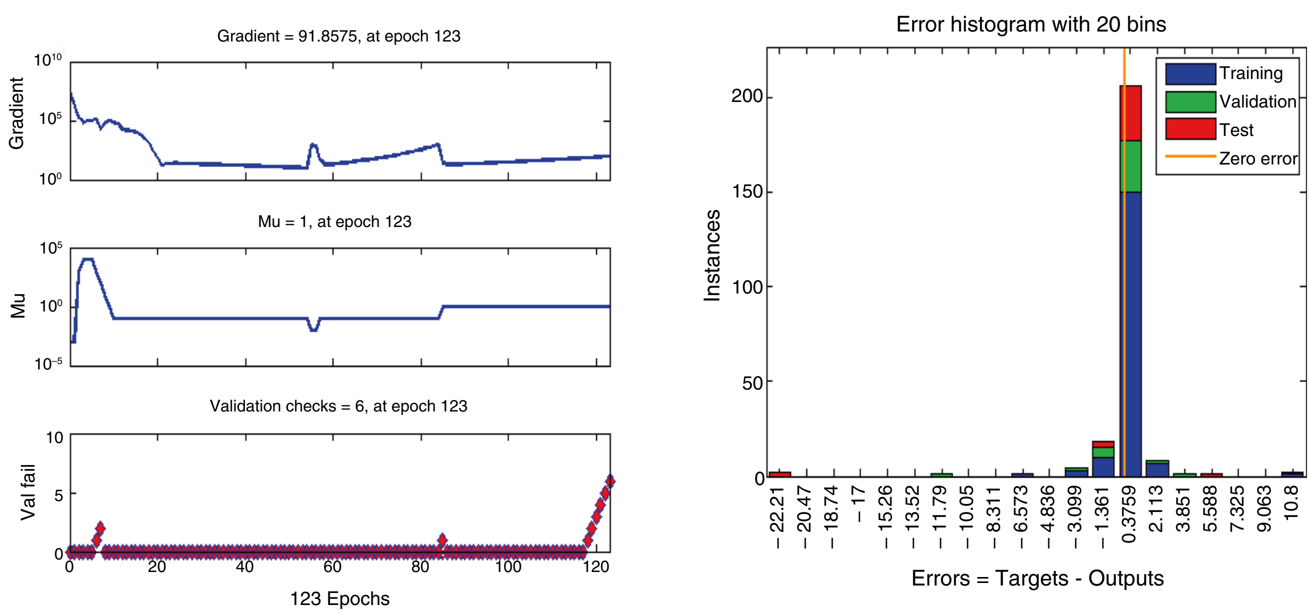

Fig. 10 Training state and error histogram graphs for parameter $\alpha = \beta = \gamma$

decays as shown in Figs. 3-5, the accuracy of model is confirmed.

3. ErrorAnalysis: LMM-ANN method is used for error analysis. Discretization error is another crucial issue.

The Fit graphs and error histograms are evaluated in Figs. 6-11. This model is compared with published work [20] as expressed in Fig. 12.

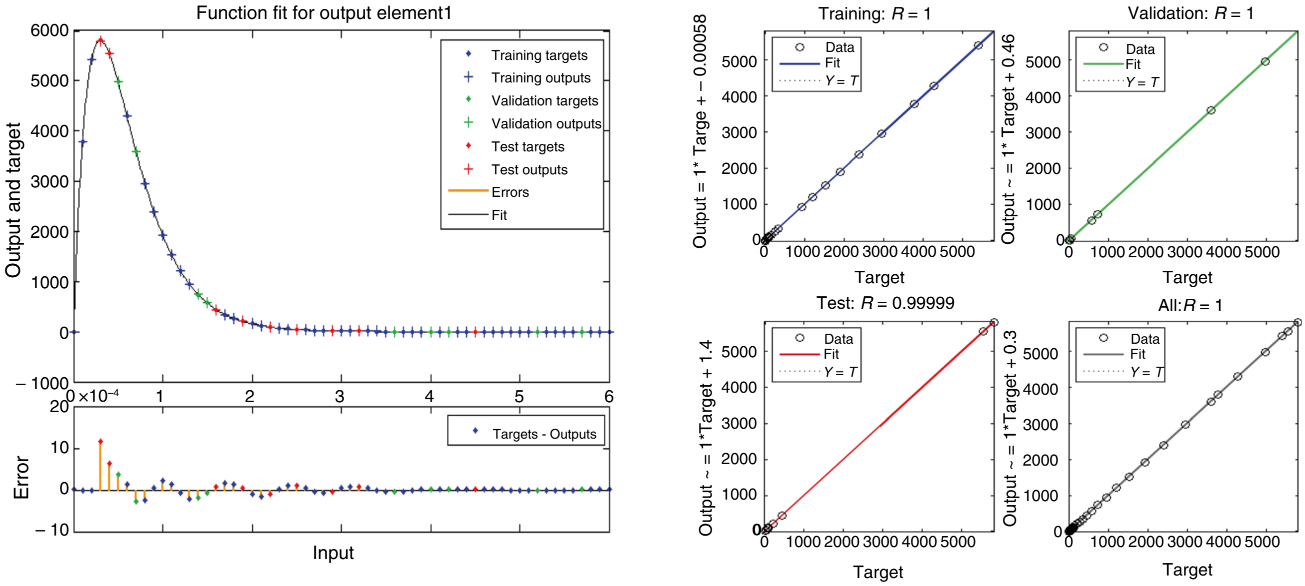

Fig. 11 Fitness and regression graphs for parameter $\alpha = \beta = \gamma$

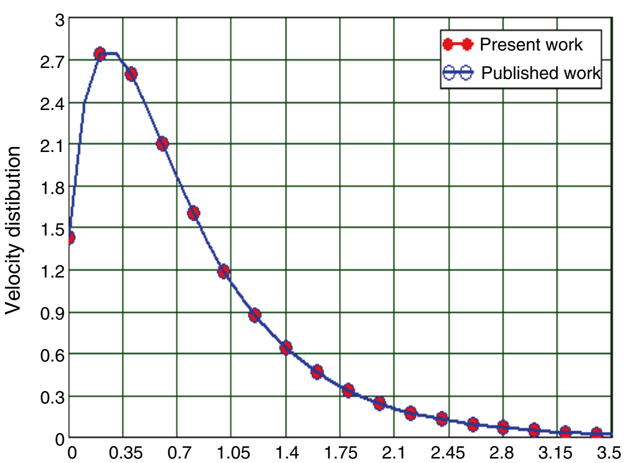

Fig. 12 Comparison of Profile of velocity

Conclusions

In the current research, brass, cobalt, titanium oxide, nickel, arsenic, and graphite nanoparticles dispersed in water were formulated as a nanofluid model in the theoretical framework of the Prabhakar fractional derivative. This model represents a complex model for the integration of mass and thermal diffusion, chemical reactions, exothermic processes and effects of porous media, thus providing a generalized methodology for analysis of complex transport phenomena. The constituent fractional-order governing equations are solved analytically using Laplace transform combined with powerful numerical methods, which further leads to a hybrid analytical-numerical method with good accuracy and high computational efficiency.

Key findings and implications

- The fluid velocity decreases with the fractional parameters ($\alpha = \beta = \gamma$), highlighting the preponderance of the memory effects introduced by the fractional operators, which is of important consequence in the design process of engineers.
- Temperature profiles show a decrease trend with increased fractional values and therefore emphasize the importance of thermal diffusion mechanisms, in accordance with Fourier's law.
- It is seen also that the concentration distributions decrease with increasing values of fractional parameter, reflecting the reduced transport memory and the non-local effects.
- Numerical evaluation confirms the reliability of the proposed methodology, while the validation is done with MATHCAD, mean-squared error analysis and regression diagnostics.
- The data are divided as 15% for testing data, 15% for validation data, and 70% for training data in the current flow model.

Limitations

The present study is based on constant thermophysical properties and idealized boundary conditions. Variations of nonlinear property behavior, transient boundary effects and more complex interactions have not been considered.

Future directions

Subsequent research should extend the model to include non-Newtonian nanofluids with spatially and temporally variable properties, inclusion of experimental verification and testing of industrial-scale applications such as heat exchangers and dynamically heterogeneous porous media applications.

Practical applications

Core practical applications of this model are:

This model has significant advantages for high-efficiency heat exchangers. Thermal transfer capability is frequently limited in conventional fluids like water and thermal oils. The incorporation of the zinc–cobalt–nickel nanoparticles increases the thermal conductivity which can be attributed to its expansive surface area and intrinsic conductivity. With its use in the industrial cooling units and radiators, this hybrid Casson nanofluid holds the potential to increase heat removal rates. The yield-stress properties of the Casson base fluid allow for better surface coating while the tri-metallic particles help enhance heat dissipation and thus more compact and energy-efficient systems.

In the field of biomedical engineering, there is a lot of potential for the model to be used for advanced drug delivery systems. Biological flow may be realistically simulated with Casson fluids because of their non-Newtonian behavior, which is comparable to that of human blood. The magnetic properties of Nickel and Cobalt nanoparticles allows to drive the nanofluid by an externally applied magnetic field. Consequently targeted drug transport to specific sites, e.g., tumorous tissue, becomes possible, reducing the side effects on the rest of the organism and increasing the precision of the therapy.

Solar energy system can also take advantage of this approach by improving thermal performance. Within direct absorption solar collectors, the working fluid is the key to the capturing and transportation of the solar heat. Zinc–cobalt–nickel nanoparticles act as efficient absorbers of solar radiation, thus increasing the energy uptake compared to conventional fluids. The inherent viscosity properties of the Casson fluid help to maintain a homogeneous particle suspension which reduces sedimentation and guarantees stable and long-term operation within collector tubes.

In high performance lubrication applications and applications with extreme mechanical requirements this model provides tangible benefits. Under the kind of loads that are typical of industrial machinery and aerospace parts, regular lubricants often lose their effectiveness. The addition of metallic nanoparticles enhances the repair of the surface by filling in the microscopic cracks, while the constituents of the solid lubricant reduce the level of friction. Moreover, the fractional formulation encapsulates the complex stress–strain response of the lubricant under abrupt loading conditions and therefore gives a better representation of the actual operation behavior.

Acknowledgements The authors extend their appreciation to the Deanship of Research and Graduate Studies at King Khalid University for funding this work through Large Research Project under Grant number RGP2/207/46.

Author contributions S. Abbas was involved in supervision; M. Ramzan contributed to investigation and methodology; R. Jan was involved in conceptualization; A. Abd-Elmonem contributed to validation; M.E.E. Abulhassan was involved in data curation; I. Khaydarov contributed to formal analysis; M. Hayitova was involved in writing original draft; I. Mahariq contributed to review and editing.

Funding None.

Data availability Data are available on request from the corresponding author.

Declarations

Conflict of interest The authors declare no conflict of interest.

References

1. Qureshi H. AI-driven analysis of buoyancy-convective flow of ternary-hybrid nanofluid in a porous medium over stretching cylinder. Nonlinear Dyn. 2025;113:28907–24.
2. Qureshi H, Zubair M, Altmeyer SA. Machine learning investigation of ternary-hybrid radiative nanofluid over stretching and porous sheet. Nanomaterials. 2025;15(19):1525.
3. Qureshi H, Altmeyer S, Zubair M. Machine learning investigation of Marangoni convection in hybrid nanofluids with Darcy Forchheimer. Sci Rep. 2025;15:1–19.
4. Qureshi H, Shah Z, Raja MA, Khan WA, Elmasry Y. Machine learning investigation through Python for thermophoretic deposition with radiation on thermal mass transfer of trihybrid nanofluid across sharp dynamics. Int J Geom Methods Mod Phys. 2025;22(07):2550027.
5. Qureshi H, Shah Z, Raja MA, Shoaib M, Khan WA, Muhammad T. Paradigm on Levenberg–Marquardt neural algorithm analysis of heat conduction optimization for ternary hybrid nanofluid with entropy generation. ZAMM J Appl Math Mech. 2024; 2024 e202301095.
6. Ramzan M, Nisa ZU, Shafique A, Nazar M. Slip and thermo diffusion effects on the flow over an inclined plate. J Adv Res Fluid Mech Therm Sci. 2022;9(2):13–28.
7. Ramzan M, Nisa ZU, Nazar M. Effect of diffusion-thermo on MHD flow of Maxwell fluid with heat and mass transfer. Front Heat Mass Transf. 2022; 12: 1-19.
8. Asjad MI, Ikram MD, Akgul A. Analysis of MHD viscous fluid flow through porous medium with novel power law fractional differential operator. Phys Scr. 2020;95:115209.
9. Krishna MV, Reddy GS. Unsteady MHD reactive flow of second grade fluid through porous medium in a rotating parallel plate channel. J Anal. 2019;27:103–20.
10. Ramzan M, Nazar M, Nisa ZU, Ahmad M, Shah NA. Unsteady free convective magnetohydrodynamics flow of a Casson fluid through a channel with double diffusion and ramp temperature and concentration. Math Methods Appl Sci. 2021;46:11322–41.
11. Haq SU, Rahman AU, Khan I, Ali F, Shah SIA. The impact of side walls on the MHD flow of a second-grade fluid through a porous medium. Neural Comput Appl. 2018;30:1103–9.

12. Sheikh NA, Ali F, Khan I, Saqib M. A modern approach of Caputo Fabrizio time fractional derivative to MHD free convection flow of generalized second grade fluid in a porous medium. Neural Comput Appl. 2018;30:1865–75.
13. Kataria HR, Patel HR. Effect of thermo-diffusion and parabolic motion on MHD second grade fluid flow with ramped wall temperature and ramped surface concentration. Alex Eng J. 2018;57:73–85.
14. Shah NA, Areshi M, Chung JD, Nonlaopon K. The new semi-analytical technique for the solution of fractional order Navier–stokes equation. J Funct Spaces. 2021;2021:1–13.
15. Sene N. Fractional model and exact solutions of convection flow of an incompressible viscous fluid under the Newtonian heating and mass diffusion. J Math. 2022;2022:1–20.
16. Das S, Jana RN. Natural convective magneto- nanofluid flow and radiative heat transfer past a moving vertical plate. Alex Eng J. 2015;54:55–64.
17. Chu Y-M, Ikram MD, Asjad MI, Ahmadian A, Ghaemi F. Influence of hybrid nanofluids and heat generation on coupled heat and mass transfer flow of a viscous fluid with novel fractional derivative. Eur Phys J Plus. 2021;144:2057–77.
18. Atangana A, Akgul A, Owolabi KM. Analysis of fractal fractional differential equations. Alex Eng J. 2020;59:1–18.
19. Atangana A, Gomez-Aguilar JF. Numerical approximation of Riemann-Liouville definition of fractional derivative: From Riemann-Liouville to Atangana-Baleanu. Numer Methods for Partial Diff Equ. 2018;34:1502–23.
20. Siyal A, Abro KA, Solangi MA. Thermodynamics of magnetohydrodynamic Brinkman fluid in porous medium. J Therm Anal Calorim. 2019;136:2295–304.
21. Ramzan M, Nisa ZU, Ahmad M, Nazar M. Flow of Brinkman fluid with heat generation and chemical reaction. Complexity. 2021;2021:1–11.
22. S. Abbas, M. Ahmad, M. Nazar, M. Amjad, H. Ali, A. Z. Jan, Heat and mass transfer through a vertical channel for the Brinkman fluid using Prabhakar fractional derivative, Applied Thermal Engineering, (2023); 232: 121065.
23. Baleanu D, Fernandez A, Akgul A. On a fractional operator combining proportional and classical differintegrals. Mathematics. 2020;8:360.
24. Chu Y-M, Ahmad M, Asjad MI, Baleanu D. Fractional model of second grade fluid induced by generalized thermal and molecular fluxes with constant proportional Caputo. Therm Sci. 2021;25:1–6.
25. Ahmad M, Imran MA, Baleanu D, Alshomrani AS. Thermal analysis of magnetohydrodynamic viscous fluid with innovative fractional derivative. Math Methods Appl Sci. 2020;24:351–9.
26. Ramzan M, Shahryar M, Abbas S, Amir M, Saydaxmetova SR, Jan R, et al. Heat transfer with magnetic force and slip velocity on non-Newtonian fluid flow through a porous medium. Partial Differ Equ Appl Math. 2025;13:1. https://doi.org/10.1016/j.padiff.2024.101033.
27. Shafique A, Ramzan M, Nisa ZU, Nazar M, Ahmad H. Unsteady Magnetohydrodynamic flow of second grade nanofluid (Ag-Cu) with CPC fractional derivative. J Adv Res Fluid Mech Therm Sci. 2022;97:2.
28. Bibi M, Zeeshan A, Malik MY. Numerical analysis of unsteady flow of three-dimensional Williamson fluid-particle suspension with MHD and nonlinear thermal radiations. Eur Phys J Plus. 2020;135(10):1–26.
29. Ramzan M, Shafique A, Abbas S, Ali R, Lamoudan T, Jan R, et al. Mathematical analysis of Prandtl number with artificial neural network and fractional operator for nanofluid flow. Case Stud Therm Eng. 2025;71(2):106164. https://doi.org/10.1016/j.csite.2025.106164.
30. Ramzan M, Shafique A, Amir M, Nazar M. Analytical solution of diffusion thermo effect on MHD second grade fluid flow with heat generation and chemical reaction through an accelerated vertical plate. Jordan J Phys. 2023;16(3):341–58.
31. Anjum A, Gaffar SA, Kumar DS, Peerusab S. Chemical radiative magnetohydrodynamics flows of micropolar nanofluid from a horizontal circular non permeable cylinder: a numerical analysis. J Nanofluids. 2025;14:95–117.
32. Anjum A, Gaffar SA, Kumar DS, Peerusab S. Computational assessment of magnetized dissipative thermo convective micropolar nanofluid flow past a rotating isothermal cone with variable temperature. Hall Curr Joule Heat J Nanofluids. 2024;13:1192–213.
33. S. Abbas, T. Saidani, M. Ramzan, S. Saleem, N. A. Othman, D. Abduvalieva, F. Benabdallahi, I. Khan, Impact of thermal radiation on fractional viscoelastic nanofluid flow with joint heat mass transfer using a neural network based approach, Journal of Radiation Research and Applied Sciences. 2025; 18 (3): 101640.
34. Anjum A, Gaffar SA, Kumar DS, Bég OA, Peerusab S. Non similar Keller box analysis of magneto chemically radiative Buongiorno's nanofluid flows past a stretching surface. J Nav Archit Mar Eng. 2024;21:127–53.
35. Parige LS, Kumar DS, Anjum A. Slow steady rotation of a spheroid in an incompressible micropolar fluid under Stokesian assumption. In: AIP Conference Proceedings. 2023.
36. Lakshmi BN, Dharmaiah G, Samdani AA, Naheed M. Influence of Darcy–Forchheimer hybrid nanofluid flow with magnetohydrodynamic and viscous dissipation effects past a permeable stretching sheet: a numerical contribution, multiscale and multidisciplinary modeling. Exp Des. 2025.
37. Anjum A, Maheswari C, Lakshmi BN, Ramana RM, Peerusab S, Gaffar SA. Computational study of magnetized 3d revolving hybrid nanofluid with non linear thermal radiation and heat source/sink over a stretching sheet, multiscale and multidisciplinary modeling. Exp Des. 2025.
38. Galal AM, Anjum A, Zafar SS, Faizan M, Zaib A, Ali F, et al. Computational assessment of chemically reactive tangent hyperbolic ternary hybrid nanofluid and thermal radiation in a Darcy-Forchheimer regime. J Radiat Res Appl Sci. 2025;18(2):101397.
39. Gaffar SA, Bég OA, Reddy PR, Anjum A, Bég TA, Kuharat S. Numerical analysis of radiative magnetoviscoelastic micropolar flow external to a sphere with a convective boundary surface condition. Heat Transf. 2025;54(5):3112–33.
40. Mehmandoosti MM, Kowsary F. Artificial neural network-based multi-objective optimization of cooling of lithium-ion batteries used in electric vehicles utilizing pulsating coolant flow. Appl Therm Eng. 2023;219:119385.
41. Blair GS, Caffyn J. Significance of power law relation in rheology. Nature. 1955;155:171–2.
42. Povstenko Y. Fractional thermoelasticity, solid mechanics and its applications. New York: Springer; 2015. p. 1–219.
43. Hristov J. Derivatives with non-singular kernals, From the Caputo-Fabrizo definition and beyond, appraising analysis with emphasis on diffusion model, Frontiers in fractional calculas. 1st ed. Sharjah: Bentham Science Publishers; 2017. p. 269–340.
44. Abbas S, Ahmad M, Nazar M, Saleem S, Isyanov R, Aljedani J, et al. Artificial neural network analysis of heat and mass transfer in fractional Casson flow. Case Stud Therm Eng. 2025;69:105946.
45. Tzou DY. Macro to microscale heat transfer, the lagging behavior. Washington, District of Columbia: Taylor and Francis; 1997. p. 01–339.
46. Stehfest H. Algorithm 368: numerical inversion of Laplace transform. Commun Adv Composit Material. 1970;13:47–9.

Authors and Affiliations

Shajar Abbas[1,2] · Muhammad Ramzan[3] · Rashid Jan[4] · Assmaa Abd-Elmonem[5] · Mawadda E. E. Abulhassan[5] · Ilkhom Khaydarov[6] · Mehrigul Hayitova[7] · Ibrahim Mahariq[8,9,10,11,12]

✉ Shajar Abbas
shajarabbasgat@gmail.com

Ibrahim Mahariq
ibmahariq@gmail.com

[1] Department of Mathematics, Saveetha School of Engineering, Saveetha Institute of Medical and Technical Sciences, Saveetha University, 602105 Chennai, Tamil Nadu, India

[2] Departnent of Computer Engineering, Biruni University, 34010 Istanbul, Turkey

[3] Centre for Advanced Studies in Pure and Applied Mathematics, Bahauddin Zakariya University, Multan , Pakistan

[4] Department of Mathematics, College of Science, Qassim University, 51452 Buraydah, Saudi Arabia

[5] Department of Mathematics, College of Science, King Khalid University, 61413 Abha, Saudi Arabia

[6] School of Exact Sciences, National Pedagogical University of Uzbekistan named after Nizami, Tashkent, Uzbekistan

[7] Department of Medicine, Termez University of Economics and Service, Termez, Uzbekistan

[8] College of Engineering and Architecture, Gulf University for Science and Technology, Mishref, Kuwait

[9] Department of Electrical and Electronic Engineering, Faculty of Engineering and Architecture , Istanbul Gelisim University, 34310 Avcılar- Istanbul, Istanbul, Türkiye

[10] Najjad Zeenni Faculty of Engineering, Al-Quds University, Jerusalem, Palestine

[11] Department of Medical Research, China Medical University Hospital , China Medical University, Taichung, Taiwan

[12] University College, Korea University, 02481 Seoul, South Korea